Dehydrogenation of homocyclic liquid organic hydrogen carriers (LOHCs) over Pt supported on an ordered pore structure of 3-D cubic mesoporous KIT-6 silica

Chang-Il Ahn [a], Yeonsu Kwak [a], Ah-Reum Kim [a], Munjeong Jang [a,b], Arash Badakhsh [a,c], Junyoung Cha [a], Yongmin Kim [a], Young Suk Jo [a], Hyangsoo Jeong [a,b], Sun Hee Choi [a,b], Suk Woo Nam [a,d], Chang Won Yoon [e,*], Hyuntae Sohn [a,b,**]

[a] Center for Hydrogen and Fuel Cell Research, Korea Institute of Science and Technology (KIST), Seongbuk-gu, Seoul 02792, Republic of Korea
[b] Energy and Environment Technology, KIST School, Korea University of Science and Technology, Seoul 02792, Republic of Korea
[c] Mechanical Design Engineering, Jeonbuk National University, Deokjin-gu, Jeonju-si 54896, Republic of Korea
[d] Green School, Korea University, Seongbuk-gu, Seoul 02841, Republic of Korea
[e] Chemical Engineering, Pohang University of Science and Technology (POSTECH), Nam-gu, Pohang-si 37673, Republic of Korea

ARTICLE INFO

ABSTRACT

Pt supported on ordered mesoporous silica (KIT-6) catalyst was examined for the dehydrogenation of homocyclic liquid organic hydrogen carriers (LOHCs, 1: MCH, 2: hydrogenated biphenyl-based eutectic mixture (H-BPDM)) conditions. The longer pore-residence time of the MCH molecules in the 3D bicontinuous pore structure of the Pt/KIT-6 catalyst strongly affected the catalytic activity because a higher MCH concentration was achieved in the vicinity of the Pt active sites. Pt/KIT-6 catalyst exhibited a higher surface area, pore volume, and Pt dispersion with narrower particle size distribution (average Pt particle size: ~1.3 nm). Therefore, higher LOHC conversion with faster hydrogen production occurred, with a higher hydrogen selectivity over Pt/KIT-6 compared with Pt/SiO$_2$ and Pt/Al$_2$O$_3$. Long-term experiment results indicated that the Pt/KIT-6 catalytic activity was stable over the reaction time than that of the other catalysts. No significant structural collapse occurred in KIT-6 during the dehydrogenation. Carbon coking was observed for all three samples.

1. Introduction

Hydrogen economy refers to a possible future energy infrastructure using hydrogen as the predominant energy carrier, leaving a zero carbon footprint [1,2]. This idea has been proposed and attracted significant attention worldwide; thus, rapid development of hydrogen-related technologies, such as water electrolysis, fuel cell and hydrogen combustion engines, have progressed rapidly [3,4]. Although various environmentally friendly hydrogen production methods to replace the current fossil fuel-based processes have been established [5], hydrogen transportation to the end-user location (e.g., hydrogen station, fuel-cell-powered building) is still challenging because of the low volumetric density of hydrogen (1 atm, 0 °C, 2.97 Wh L^{-1}). Along with compressed and liquified hydrogen storage techniques, liquid organic hydrogen carriers (LOHCs) are promising hydrogen storage materials

that can transport large quantities of hydrogen because of the high hydrogen storage density (5–7 wt%) and chemical/physical stability at ambient temperature and pressure and high commercial availability [6–9]. LOHCs are also expected to be compatible with conventional fuel infrastructure because of the inherent properties of fossil fuels. Therefore, the cycle of hydrogen storage via hydrogenation, production by dehydrogenation, and utilization using LOHCs have recently attracted much interest in hydrogen research communities.

Among many other molecules, homoaromatic LOHCs, including MCH (6.2 wt% hydrogen storage) [10–12], perhydro-dibenzyltoluene (H18-DBT, 6.2 wt%) [9,13,14], bicyclohexyl (7.3 wt%) [15,16], and heteroaromatic perhydro-*N*-ethylcarbazole (H12-NEC, 5.8 wt%) [17, 18], have been studied and tested on a large scale. A biphenyl-based eutectic mixture (BPDM, 35 wt% biphenyl and 65 wt% diphenyl-methane, 6.9 wt% hydrogen storage) has also been developed as a viable

option to maximize the gravimetric hydrogen storage capacity [19,20]. For both the hydrogenation and dehydrogenation processes of these compounds, a well-designed catalyst is required to store and release hydrogen at a stable high rate with minimal by-product formation. In particular, dehydrogenation reaction occurs at higher temperatures (> 250 °C) compared with the hydrogenation processes and often results in severe coking on the catalyst surface. Thus, achieving high catalytic activity, selectivity, and durability at these dehydrogenation temperatures is an ongoing challenge [21–23].

Pt is the most active metal known for LOHC dehydrogenation, and this is attributed to its high activity for C-H bond cleavage [7,24]. In particular, Pt supported on alumina (Al_2O_3) with high metal-support interactions has been reported in the literature, as demonstrating promising catalytic activity and stability for LOHC dehydrogenation [7, 25,26]. The strong metal-support interaction of the Pt/γ-Al_2O_3 catalyst facilitates hydrogen spillover, helping the reaction equilibrium to move favorably toward the production of toluene and hydrogen [27]. However, in many cases, the acidic surface of Al_2O_3 accelerates catalytic deactivation via various undesirable side reactions, such as coke formation [28,29], isomerization [29], and catalytic cracking [30,31]. Studies have reported that the acidic surface sites are related closely to the cracking and isomerization of the reactant and therefore, coking on the catalyst surface [32], for LOHC dehydrogenation reactions. For example, Usman et al. [29] reported that ring-closed products, such as ethylcyclopentane and dimethylcyclopentanes, are intermediate species produced via isomerization over the acidic sites of the Pt/γ-Al_2O_3 catalyst for MCH dehydrogenation. The cyclopentadienes derived from these by-products eventually transform to coke on the catalyst surface, as well as the Pt active sites via polymerization, resulting in low catalytic activity and selectivity toward toluene [28,29,31].

The extent of side reactions can be controlled by altering the chemical and/or physical characteristics of the active sites. For MCH dehydrogenation, the strategy of adding a second metal (e.g., Re) was extensively studied from the 1970 s to the early 2000 s because of the reported superior activity of Pt-Re/Al_2O_3 catalyst compared with Pt/ Al_2O_3 [26,33]. Pt-Re catalyst exhibited a faster MCH dehydrogenation rate and higher toluene selectivity, which was attributed to the enhanced desorption of the products and hydrogen from the catalyst surface (change in the rate-determining step [26]). More recently, Nakano et al. [34] reported other bimetallic catalysts, e.g., Pt-Mn, where the incorporation of Mn reduced the unsaturated coordination of Pt, resulting in higher toluene selectivity and tolerance for coke formation. Okada et al. successfully operated a pilot-scale MCH dehydrogenation unit (hydrogen generation rate > 1000 $Nm^3/h/m^3$ cat) for 6000 h at an MCH conversion > 95% and toluene selectivity > 99.9% (593 K, liquid hourly space velocity (LHSV) 2.0 h^{-1}) [10]. In this instance, alkali metal was added to Pt (Pt-K/Al_2O_3) to reduce the acidity of the catalyst. The extent of electron density of the surrounding active sites was found to be a determining factor for catalytic activity [35] in the LOHC dehydrogenation reaction. Furthermore, a wide range of experimental and theoretical studies on LOHC dehydrogenation have been extensively conducted recently [35–48].

In addition to Al_2O_3, SiO_2-based materials, such as ordered mesoporous silica (OMS) with a hierarchical structure, have many advantages as a support: 1) relatively larger pore size than zeolites, 2) high surface area, and 3) regular pore structure. OMS was first developed as an alternative to zeolite by researchers at the Mobil Corporation for catalyst supports [49–53]. Many different types of OMSs have been synthesized because of their relatively convenient synthetic procedures and reproducibility [54]. SBA-15 and KIT-6, which are major OMSs, are widely utilized as catalyst supports and hard templating materials for a variety of heterogeneous catalytic applications (e.g., oxidation [55–60], esterification [61], hydrogenation [62], and dehydrogenation [63–65]).

To the best of our knowledge, Pt supported on OMS catalysts has not been extensively investigated for its reactivity in LOHC dehydrogenation, except for a few studies on decalin dehydrogenation conducted by

Martynenko et al. [65]. The authors investigated the catalytic reactivity of Pt/SBA-15 and Pt/MCM-48 in decalin dehydrogenation and claimed that the enhanced decalin conversions achieved over Pt/OMS catalysts were strongly related to the high Pt dispersion of the catalyst (as high as 70%). Furthermore, the growth of Pt nanoparticles inside the mesopores was limited, possibly because of the confinement effect of the OMS structure, thus improving the stability of the catalyst under the reaction conditions. Regular silica (SiO_2)-supported catalysts have been studied in recent research [22,65]. However, these studies focused more on the characteristics of the active site rather than on the pore structure-activity relationship.

Herein, Pt catalysts supported on KIT-6 were synthesized and tested for the dehydrogenation of homocyclic LOHCs (1: MCH, 2: hydrogenated biphenyl-based eutectic mixture (H-BPDM)). Their catalytic activities were compared with those of the Pt/SiO_2 and commercial Pt/ Al_2O_3 catalysts. It should be noted that KIT-6 with an ordered 3-D cubic pore structure has never been investigated as a catalyst support for LOHC dehydrogenation. Multiple characterization techniques, including physi/chemisorption, X-ray spectroscopy, and transmission electron microscopy, were utilized to identify the pore structure, surface area, particle size, metal dispersion, surface acidity, and metal oxidation state of the catalysts. The effect of the ordered pore structure of KIT-6 on the catalytic activity and selectivity is demonstrated in detail. A post-catalysis analysis was conducted to understand catalyst deactivation under the reaction conditions.

2. Experimental

2.1. Material preparation

Amorphous silica (SiO_2, Alfa-Aesar) and Pt/Al_2O_3 (1.0 wt%) catalyst (denoted by Pt/Al_2O_3, Sigma-Aldrich) were purchased and used without further purification as reference materials; they were used as a support and a commercial catalyst for LOHC dehydrogenation, respectively. Pluronic P123 (MW ~5800, Sigma-Aldrich), hydrochloric acid (37% solution in water, ACROS), 1-butanol (99.4%, Sigma-Aldrich), and tetraethoxysilane (TEOS, 99.0%, Alfa-Aesar) were purchased and used to synthesize KIT-6, without any further purification. MCH (Samchun Chemical, 99.0%) was purchased and used as a reactant for LOHC dehydrogenation. Additionally, biphenyl (($C_6H_5)_2$, Sigma-Aldrich), and diphenylmethane (($C_6H_5)_2CH_2$, Tokyo Chemical Industry) were mixed, then hydrogenated to prepare H-BPDM (35 wt% bicyclohexyl and 65 wt % dicyclohexylmethane) as reported in earlier papers [19,20]. Finally, tetraammineplatinum (II) nitrate ([Pt($NH_3)_4](NO_3)_2$, Alfa-Aesar) was used as the Pt precursor for all the prepared catalysts.

2.2. Catalyst synthesis

2.2.1. Synthesis of OMS

KIT-6 was prepared by referring to previously reported soft templating and hydrothermal methods [37–42]. The $EO_{20}PO_{70}EO_{20}$ triblock copolymer (Pluronic P123, Sigma-Aldrich, 16.0 g), which served as a structure-directing agent for making highly regular ordered mesoporous structures, was first fully dissolved in 150 mL of deionized water (DIW). The solution was then mixed with dilute hydrochloric acid (25 mL of 37% HCl solution) with gentle stirring (200 rpm) at 35 °C until a homogeneous solution was obtained, after which 16.0 g of 1-butanol was added, and the mixture was stirred for 1 h at 35 °C. Finally, 34.4 g of TEOS, a silica source, was added and stirred vigorously for 24 h at 35 °C. The resulting solution was poured into a Teflon-lined stainless-steel autoclave and aged for 25 h at 110 °C under static conditions. The final solution was filtered by vacuum filtering, and the collected white precipitate was dried in a convection oven at 110 °C. The obtained silica powder was treated with hydrochloric acid/water/ethanol solution under mild stirring (2 h) to extract a portion of the used copolymer and rinsed several times with deionized water until a pH of 7 was reached.

The resulting silica powder was dried at 110 °C and calcined at 550 °C for 6 h under static air conditions at a ramp rate of 1 °C/min to obtain KIT-6.

2.2.2. Synthesis of 1 wt% Pt loaded LOHC dehydrogenation catalysts

Pt of 1 wt% was successfully added on KIT-6 and SiO_2 by wet impregnation using a rotary evaporator. In detail, a calculated amount of the Pt precursor (1 wt% of Pt loading by total catalyst weight percent) was dissolved fully in DIW and poured into the silica-based supports. The metal salt solution-support powder slurry was agitated repeatedly in a rotary evaporator at 25 °C for 2 h under mild vacuum conditions (311 Torr) to remove oxygenated species from the catalysts and to ensure the precursor solution penetrated well into the mesopores. The solvent was then evaporated by increasing the bath temperature (30–35 °C) under mild vacuum conditions (160 Torr) for approximately 0.5 h and then dried at 80 °C overnight. The resulting dried catalyst powder was calcined at 450 °C for 3 h at a ramp rate of 1 °C/min. The catalysts prepared for LOHC dehydrogenation are denoted by Pt/KIT-6 and Pt/SiO_2.

2.3. Catalyst characterizations

2.3.1. Inductively coupled plasma optical emission spectroscopy (ICP-OES)

The Pt loadings of all the catalysts were measured by ICP-OES using an OPTIMA 5300DV, PerkinElmer. All the catalyst samples were pretreated with HCl, HF, and HNO_3 prior to analysis using the acid digestion method. The weight percentage of Pt was quantified from a calibration curve obtained using a standard Pt ICP solution.

2.3.2. N_2 physisorption

The surface area, total pore volume, and average pore size were obtained via N_2 physisorption (ASAP 2000, Micromeritics, USA) based on the Brunauer Emmett Teller (BET) and Barrett Joyner Halenda (BJH) methods. All the samples were first degassed at 350 °C under vacuum (< 30 mm Hg) overnight to remove any impurities on the catalyst surface. N_2 adsorption and desorption over the samples were analyzed at −196 °C.

2.3.3. Scanning/transmission electron microscopy (STEM)

The microstructure and surface morphologies of the fresh and used catalysts were observed by TEM (TitanTM80–300, FEI transmission electron microscope instrument operated at 200 kV). High-angle annular dark-field imaging (HAADF) in the STEM mode was performed to determine the size distributions of the Pt nanoparticles (NPs) and to investigate the change in Pt particle size during the dehydrogenation reactions. Post-imaging analysis was performed using an image processing program distributed by the National Institutes of Health (USA), ImageJ.

2.3.4. Chemisorption of NH_3, O_2, CO, and H_2

Ammonia temperature-programmed desorption (NH_3-TPD) was performed to identify the acidic properties of the catalysts using an automated catalyst characterization system (AutoChem II 2920, Micromeritics, USA) equipped with a thermal conductivity detector (TCD). First, the catalyst sample was pretreated at 600 °C for 1 h under a He atmosphere to remove water molecules and organic impurities. NH_3 adsorption was performed under an NH_3/He (15%) flow (50 mL/min) at 100 °C for 30 min, after which the physisorbed NH_3 was flushed under pure He. NH_3 desorption analysis was conducted (100–950 °C) at a heating rate of 10 °C/min and flow (50 mL/min) of pure He. The desorbed NH_3 from the effluent gas was evaluated quantitatively using TCD.

Temperature-programmed oxidation (TPO) was performed to analyze the quantity of coke deposited on the catalyst surface during the dehydrogenation (AutoChem II 2920, Micromeritics, USA). The samples were pretreated with pure He at 120 °C for 1 h. For the TPO analysis, O_2/

He (5%, 100 mL/min) was supplied, while the temperature was increased from 100 °C to 800 °C at 10 °C/min. The reactor temperature was then maintained at 800 °C for 15 min to ensure complete oxidation of the coke-deposited spent catalysts.

CO chemisorption (CO-Chemi) was performed to clarify the dispersion of the active metal (Pt) of each catalyst (AutoChem II 2920, Micromeritics, USA). Before CO-Chemi, the catalyst sample was reduced under pure H_2 at 400 °C for 30 min. It was then purged with pure Ar at 400 °C for 30 min. Finally, CO-Chemi analyses were performed at 50 °C with periodic injection of CO/He (10%, 1 mL) for 4 min. For a simple estimation, the adsorption stoichiometric ratio of CO/Pt (mol/mol) was fixed set to 1.

Finally, the reducibility of each catalyst was confirmed via temperature-programmed reduction (TPR) experiments. Each catalyst was pretreated under a pure Ar atmosphere at 200 °C for 1 h and then reduced from 100 °C to 700 °C (10 °C/min) under a flow of H_2/Ar (10%, 25 mL/min).

2.3.5. In situ diffuse reflectance infrared Fourier transform spectroscopy (DRIFTS): adsorption/desorption of methylcyclohexane (MCH)

The in situ DRIFTS analysis was performed to understand the adsorption and desorption characteristics of MCH molecules over the Pt-based catalyst surface. The experiment was performed using a Fourier transform infrared (FT-IR) spectrometer (Nicolet iS10, Thermo Fischer Scientific, USA) equipped with an MCT/A detector and a high-temperature reaction chamber (Praying Mantis™) sealed with a domed stainless-steel cover. The powder catalysts were first finely ground and loaded into the reaction chamber. The samples were purged with N_2 and pre-reduced at 400 °C for 30 min under continuous pure H_2 flow. The temperature of the reaction chamber was then reduced to 25 °C under an N_2 atmosphere. Saturated MCH vapor was generated using a bubbler system and filled (using a carrier gas (N_2)) into the reaction chamber at room temperature for 1 h. Once the adsorption was complete, the sample was flushed with pure N_2 to remove the physically adsorbed MCH molecules. The reaction chamber was heated to 100 °C under pure N_2. At this temperature, DRIFTS spectra were obtained repeatedly at 3 min intervals while flushing the samples with N_2. The entire process was repeated at 200 °C. Once the MCH desorption was complete, the MCH vapor was again introduced into the DRIFTS cell at 300 °C for 1 h. For this experiment, the MCH vapor constantly flowed into the reaction chamber, while the DRIFTS spectra were collected repeatedly at 5 min intervals for 30 min. During the entire experiment, a background spectrum was collected and subtracted from the sample for each step.

2.3.6. X-ray absorption near edge spectroscopy (XANES)

XANES analysis was conducted on *ex situ* reduced Pt-based samples to estimate the oxidation state of Pt. *Ex situ* XANES spectra were collected at the 10 C beamline (wide X-ray absorption fine structure (XAFS)) at the Pohang Accelerator Laboratory (PAL) located in Pohang, South Korea. The beamline can provide photon energy in the range of 4–60 keV using a Si (111) and Si (311) double crystal monochromator. All the samples were finely ground prior to the experiment to improve sample homogeneity. The collected spectra at the Pt L_3-edge (11,564 eV) were analyzed using Athena software, where the quantification of the Pt oxidation state was performed by the linear combination of the spectra of Pt metal foil and that of the PtO_2 standard.

2.4. Catalytic activity tests

The LOHC dehydrogenation activity of each Pt catalyst was evaluated using an identical testing protocol [25]. The sample (1.0 g, Pt/KIT-6, Pt/Al_2O_3, and Pt/SiO_2) was loaded in a lab-scale fixed bed tubular reactor with an outer diameter (O.D., stainless-steel) of 1/2', in which the catalysts were supported by quartz wool. Prior to the experiment, each catalyst was reduced under a flow of pure H_2 at 400 °C for

30 min. The reactor was then cooled to the reaction temperature (H-BPDM at 340 °C and MCH at 300 °C), and the reactants were sent to the reactor mixed with co-fed H_2 at a fixed molar ratio of H_2/LOHC (from 1.90 to 2.05: H-BPDM & 0.019: MCH). The reactor entrance (LOHC inlet, liquid phase) was preheated to ensure that the reaction occurred in the gas phase. The LHSV varied from 1.2 to 3.6 mL/g_{cat}/h and the reaction pressure was fixed at atmospheric pressure for all experiments. Catalytic durability tests were performed for approximately 20 h at 340 °C (H-BPDM) and 300 °C (MCH) after testing for changes in the space velocity (mL/g cat./h). The dehydrogenation liquid products were collected with a vapor-liquid separator, and the separated gas products were passed through a molecular sieve 13X column to remove any leftover organic species. The column outlet was connected to an H_2 mass flow meter (H_2-MFM, F-201CL, Bronkhorst) to accurately measure the H_2 flow rate. The degree of dehydrogenation (DoDH) was defined based on Eq. (1). The theoretical H_2 production was determined assuming that the reactant converted completely to its dehydrogenated form.

Qualitative and quantitative analyses of the liquid hydrocarbon products and their compositions were performed using gas chromatography-mass spectroscopy (GC-MS, GC: 6890 N GC System, Agilent, USA, TOF-MS: Pegasus IV, LECO, USA with column DB-5MS ($30 \times 0.25 \times 0.25$), Agilent, USA); the oven temperature was increased from 40 °C to 280 °C at 10 °C /min.

Degree of $Dehydrogenation(\%, DoDH)$

$$= \frac{\text{Measured } H_2 \text{ production } \left(\frac{mL}{min}\right)}{\text{Theoretical } H_2 \text{ production } \left(\frac{mL}{min}\right)} \times 100 \qquad (1)$$

3. Results and discussion

3.1. Characteristics of prepared Pt-based LOHC dehydrogenation catalysts

The specific surface area, total pore volume, and average pore diameter of the Pt-based catalysts are listed in Table 1. It is widely known that the ordered mesoporous structure has a relatively higher surface area and total pore volume, and a narrower pore size distribution compared with other metal oxides. The BET surface area and total pore volume decreased in the order of Pt/KIT-6 > Pt/SiO$_2$ > Pt/Al$_2$O$_3$. Pt catalysts supported on KIT-6 exhibited a significantly higher specific surface area (847 m^2/g) and pore volume (1.18 cm^3/g) than other catalysts. N_2-isotherm-type IV curves with typical hysteresis loops for the ordered mesoporous structure were obtained for the Pt/KIT-6 catalysts (Fig. 1a), indicating the presence of uniform mesopores. The pore size distributions of Pt/KIT-6 revealed that nearly all the mesopores have a uniform diameter of 5–6 nm (Fig. 1b). The Pt weight loading in the as-synthesized catalysts fell into a narrow range of 1.0 wt% ± 0.11, as expected.

The microstructures of the as-prepared catalysts were observed by electron imaging (Fig. 2). The Pt particle size distributions were acquired from multiple HAADF-STEM images of the as-prepared Pt

Fig. 1. (a) N_2 adsorption-desorption curves and (b) pore size distributions of Pt/Al$_2$O$_3$, Pt/SiO$_2$ and Pt/KIT-6 catalysts.

catalysts and plotted as histograms. Pt/KIT-6 has a well-developed ordered mesoporous structure with uniform mesopores of 5–6 nm (Fig. 2a1 and 2a2). The morphology of the Pt NPs was polyhedral for all samples. In comparison with Pt/SiO$_2$ and Pt/Al$_2$O$_3$, the Pt NPs supported on KIT-6 are smaller and more highly monodispersed. As shown in the particle size distribution, the curve is excessively narrower for Pt/KIT-6, possibly suggesting that the formation of Pt particles was confined due to the well-ordered mesopore structure. The size of the Pt particles, formed on each support, was in the order of Pt/SiO$_2$ > Pt/Al$_2$O$_3$ > Pt/KIT-6. The reactant accessibility to these Pt particles was different as per the CO chemisorption results (Table 1 and Fig. S1). A Pt dispersion of 44% was measured over Pt/KIT-6. This value was higher than those of the Pt/SiO$_2$ and Pt/Al$_2$O$_3$ catalysts, which do not have a regular mesopore structure.

Table 1
Textural and mechanical properties of the as-prepared Pt/Al$_2$O$_3$, Pt/SiO$_2$, and Pt/KIT-6 catalysts.

Catalyst	S_B[a] (m^2/g)	V_t[a] (cm^3/g)	D_p[a] (nm)	Pt loading[b] (wt%)	Dispersion[c] (%)	$D_{p,\,STEM}$[d] (nm)
Pt/KIT-6	846.8	1.179	5.741	0.891	44.03	1.310
Pt/SiO$_2$	265.7	1.008	13.101	0.912	33.69	2.222
Pt/Al$_2$O$_3$	105.7	0.265	7.308	1.0[e]	37.58	2.164

[a] N_2 physisorption was performed on the fresh catalysts; the abbreviations S_B, V_t, and D_p represent the specific BET surface area (m^2/g), total pore volume (cm^3/g), and average pore diameter (nm), respectively.
[b] Pt loading was obtained from ICP-OES.
[c] Pt dispersion was determined by pulse CO chemisorption.
[d] Averaged Pt particle sizes were acquired from STEM images.
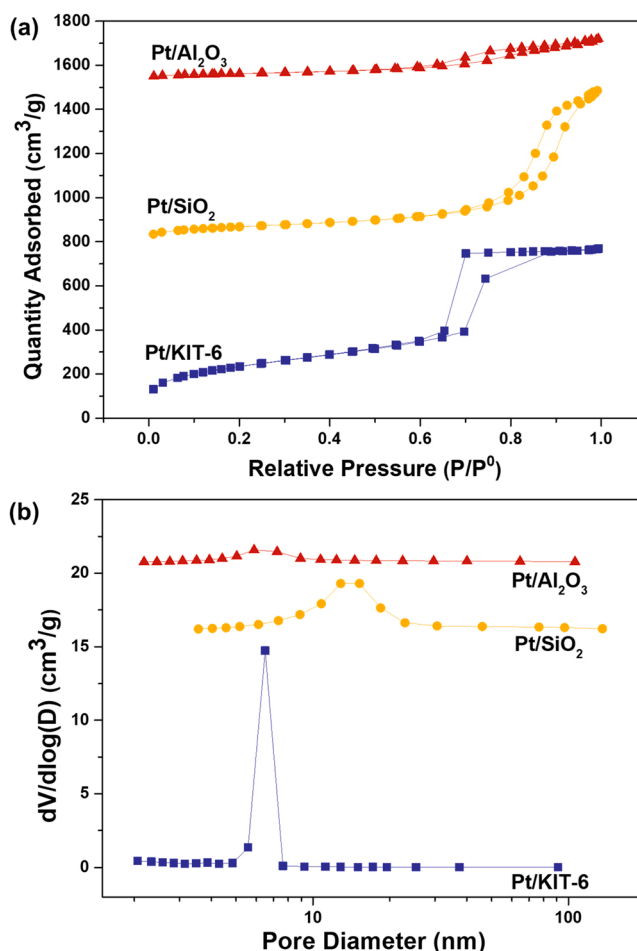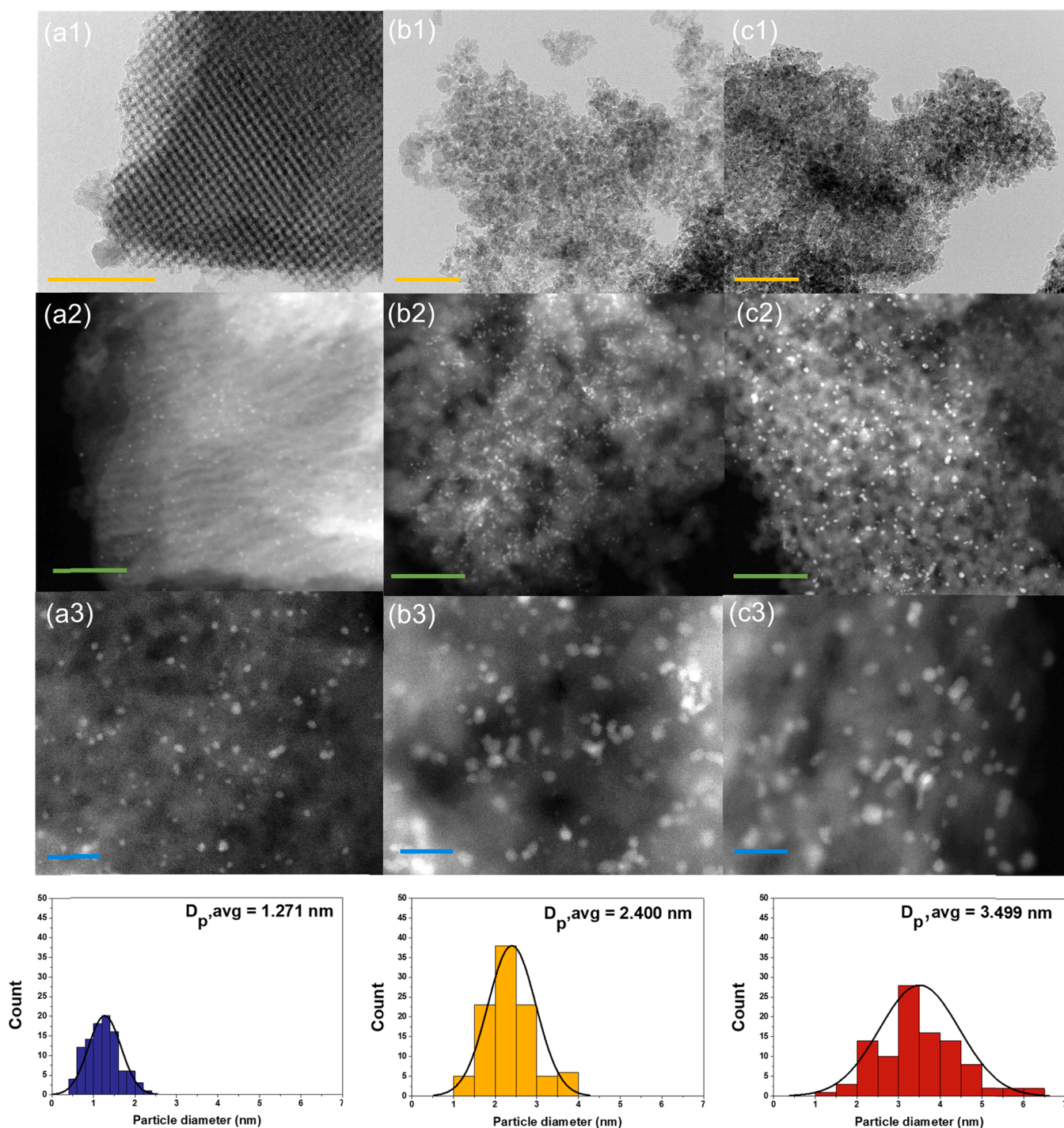[e] Manufacturer Report (Aldrich), 232,114, Lot # MKCF9123.

Fig. 2. TEM (a1-c1) and STEM (a2-c3) images including Pt particle size distributions of (a) Pt/KIT-6, (b) Pt/SiO$_2$, and (c) Pt/Al$_2$O$_3$ (scale bar: yellow = 100 nm, green = 50 nm, blue = 10 nm).

3.2. Surface acidity and Pt reducibility

The NH$_3$-TPD results for the qualitative analysis of the acidic sites are presented in Fig. 3a. The strength of the acidic sites can be estimated from the NH$_3$-desorption temperature, while the number of acidic sites is generally estimated based on the area of the NH$_3$-desorption peaks. In general, the desorption peaks in the range of 100–130 °C are attributed to the desorption of physically adsorbed NH$_3$. The desorption peaks in the range of 150–300, 300–450, and 450–600 °C correspond to weak, medium, and strong acidic sites, respectively [66]. Clearly, a considerably large quantity of NH$_3$ was desorbed from Pt/Al$_2$O$_3$, which agrees

well with that quoted in the literature [67]. This revealed the high surface acidity of the Pt/Al$_2$O$_3$ catalyst. For Pt catalysts supported on KIT-6 and SiO$_2$, a negligible quantity of NH$_3$ was detected in the range of 200–300 °C. These results also indicate that these catalysts' surfaces are relatively less acidic compared with Pt/Al$_2$O$_3$. The desorption peaks of strongly acidic sites were not observed.

TPR analysis was performed to examine the H$_2$ consumption characteristics of Pt-based catalysts (Fig. 3b). A broad reduction peak was observed in the lower temperature region (< 200 °C) for the Pt/KIT-6 and Pt/SiO$_2$ catalysts, whereas a sharper H$_2$ consumption peak was observed at 440 °C for the Pt/Al$_2$O$_3$ catalyst. H$_2$ consumption peaks at
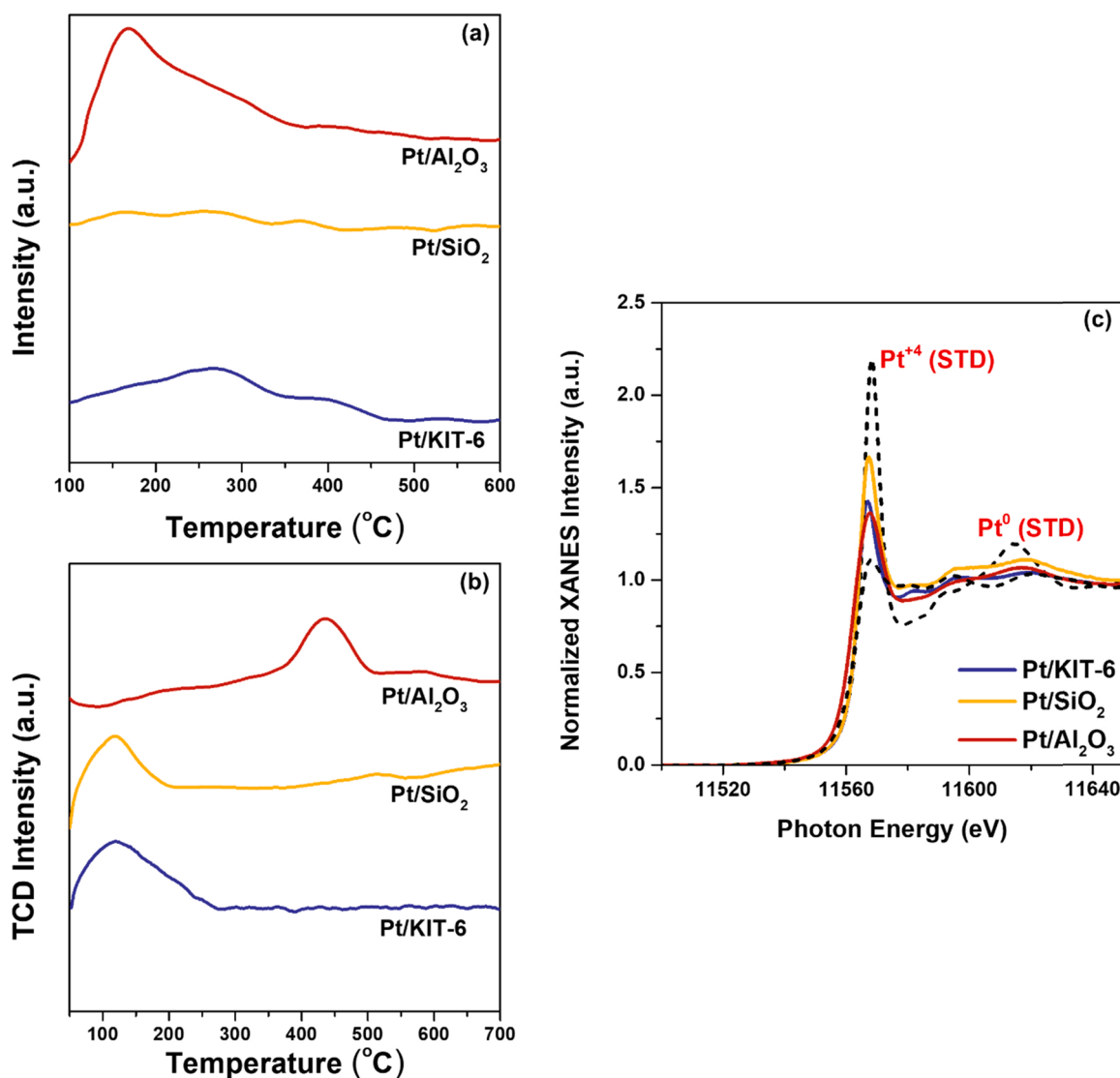
Fig. 3. Results of (a) NH$_3$-TPD, (b) TPR, and (c) *Ex situ* XANES analysis performed over Pt/Al$_2$O$_3$, Pt/SiO$_2$, and Pt/KIT-6 catalysts.

lower temperatures (100–300 °C) are generally related to the reduction of surface Pt oxide species (PtO$_x$), while the peaks at higher temperatures (350–550 °C) are related to the reduction of Pt bulk oxide strongly interacting with the catalyst support [68]. The high reduction temperature of the Pt supported on Al$_2$O$_3$ suggests that these Pt particles exhibit stronger metal-support interactions than those supported on SiO$_2$ and KIT-6. This was an expected result considering that SiO$_2$-based supports are fairly inert.

Furthermore, the Pt oxidation states of the *ex situ* reduced samples were measured using the XANES technique. The reduction procedures were identical to the conditions employed prior to activity testing (pure H$_2$ at 400 °C). However, the samples were exposed to air before XANES data collection. Therefore, Pt nanoparticles were moderately oxidized (Fig. 3c); the estimated oxidation states were Pt$^{+1.95}$, Pt$^{+1.12}$, and Pt$^{+1.04}$ for Pt/SiO$_2$, Pt/KIT-6, and Pt/Al$_2$O$_3$, respectively. These results indicate that the Pt particles supported on KIT-6 and Al$_2$O$_3$ are more stable than those supported on SiO$_2$ under air conditions and/or are likely to be more reducible under reducing conditions.

3.3. LOHC dehydrogenation reactivity of Pt/X (X = KIT-6, SiO$_2$, Al$_2$O$_3$)

3.3.1. Dehydrogenation of MCH to toluene

The MCH dehydrogenation activities of the catalysts were obtained at a reaction temperature of 300 °C and pressure of 1 bar (Fig. 4). The Pt/KIT-6 catalyst exhibited better catalytic activity at all the tested LHSV conditions compared with the other two catalysts (Fig. 4b). The average degree of dehydrogenation (DoDH), that is, the ratio of the actual hydrogen production rate to the theoretical value, was in the order of Pt/KIT-6 > Pt/Al$_2$O$_3$ > Pt/SiO$_2$. It should be noted that the increase in the DoDH value at 3.6 mL/g$_{cat}$/h was double that of the Pt/KIT-6 catalyst as compared with Pt/SiO$_2$, revealing that the silica-based ordered mesoporous structure has a positive correlation with the catalytic activity for MCH dehydrogenation. Moreover, a linear decrease in activity was observed for all samples with increasing LHSV. However, the decrease in DoDH for Pt/KIT-6 was significantly low (from 100% to 90%, from 1.2 to 3.6 mL/g$_{cat}$/h), whereas for both Pt/Al$_2$O$_3$ and Pt/SiO$_2$ catalysts, a greater drop in activity was observed with increasing LHSV values. This is possibly attributed to the complex 3D bicontinuous pore structure of the Pt/KIT-6 catalyst, which might increase the pore-residence time of the support matrix. That is, a higher surface reactant concentration can be reached near the Pt active sites, resulting in higher catalytic activity. Although the MCH feed rate increases, the Pt/KIT-6 catalyst retains more MCH molecules within its structure, thereby increasing the opportunities for dehydrogenation to proceed. This is demonstrated in more detail with the experimental evidence in Section 3.3.2.
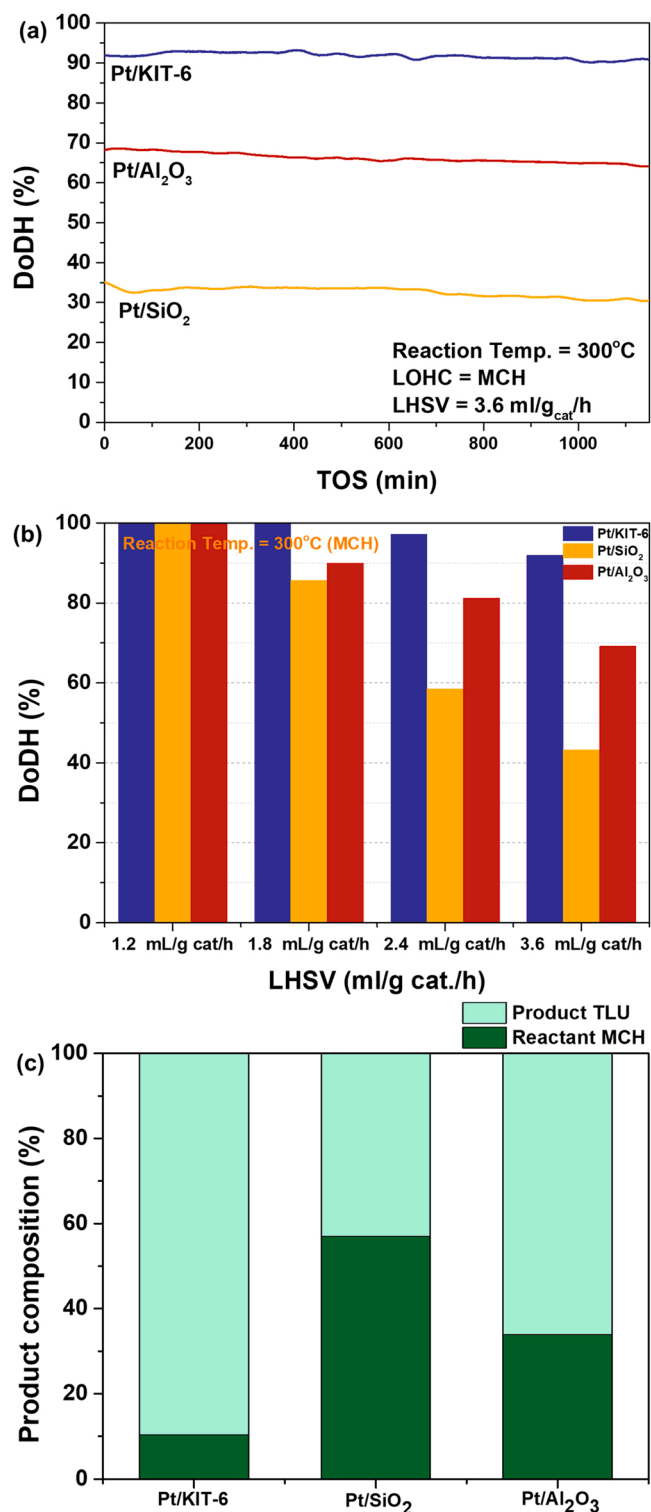
Fig. 4. Catalytic activity results for Pt/Al$_2$O$_3$, Pt/SiO$_2$, and Pt/KIT-6 catalysts under MCH dehydrogenation conditions: (a) Stability testing, (b) Reaction at varying LHSV values, and (c) Liquid product composition (TLU: toluene, MCH: methycyclohexane).

The catalytic stability of the Pt-based catalysts was further examined for approximately 20 h (Fig. 4a). A DoDH value of 92% was achieved for the Pt/KIT-6 catalyst at the beginning of the reaction and remained stable over time. However, Pt/Al$_2$O$_3$ and Pt/SiO$_2$ samples exhibited noticeable catalyst deactivation. The liquid products obtained during MCH dehydrogenation (after 15 h of reaction) were analyzed, and their compositions are displayed in Fig. 4c. Only the reactant (methyl-cyclohexane) and the product (toluene) were detected. The DoDH value (Fig. 4a) and the remaining MCH composition matched well, indicating that all the MCH molecules converted into toluene, releasing 3 mol of H$_2$ with minimal side reactions, except for coke formation (Section 3.4.).

3.3.2. Pore-residence time in KIT-6: In situ DRIFTS results

3.3.2.1. MCH adsorption at room temperature (RT). The excellent catalytic activity of Pt/KIT-6 is likely attributed to its high surface area and Pt dispersion, resulting in more accessible active Pt sites for MCH dehydrogenation. However, the differences in obtained Pt dispersion between Pt/KIT-6 and Pt/Al$_2$O$_3$ are not significant (~ 6%). Another possible explanation is the increase in MCH concentration near Pt active sites induced by the bicontinuous cubic mesoporous structure of KIT-6. It can be speculated that the increase in the pore-residence time of the reactants and products markedly increases the contact time with the Pt active sites, thus promoting LOHC dehydrogenation activity and mini-mizing the formation of partially dehydrogenated products. The ability of mesopores to capture reactants for a longer period has been demon-strated in previous studies. For example, Rottreau et al. investigated the in-pore diffusion of fatty acids within the pores of KIT-6, SBA-15, and bulk solutions [69]. The authors reported that longer chain acids were observed from the catalytic esterification of carboxylic acids because of the tortuous nature of the OMS supports. The highest esterification ac-tivity was acquired over KIT-6 and attributed to its 3D bicontinuous cubic helical structure, leading to a decrease in the diffusion coefficient and an increase in the diffusion delay time. Similarly, Prieto et al. [70] stated that an increase in pore length results in an increase in the pore-residence time. In their study, larger quantities of C5 + hydrocarbons were selectively achieved using short-pore RuCo/SBA-15 catalysts under Fischer-Tropsch synthesis conditions; this was attributed to the short-pore-residence time.

In situ DRIFTS was thus performed to understand the relative dif-ference in the pore-residence time of the catalysts by comparing the surface MCH adsorption and desorption characteristics (Figs. 5 and 6). MCH adsorption was performed at RT for 1 h and was thereafter flushed with pure N$_2$ to remove the physically adsorbed MCH molecules. The desorption spectra at RT, 100, and 200 °C, with respect to the flushing time with N$_2$, are presented in Fig. 5. Two main adsorption peaks were detected at approximately 2800–3000 cm^{-1} for all the samples. They are aliphatic C-H stretching vibrations[57]; the peaks at 2920 and 2850 cm^{-1} are related to the asymmetric and symmetric CH$_2$ modes, respectively [71]. The high peak intensity of the CH$_2$ stretching vibra-tion is reasonable because a large proportion of the MCH chemical structure consists of five -CH$_2$ groups. The contribution of the methyl group (-CH$_3$) to the MCH adsorption peak intensity can be analyzed via deconvolution of the desorption spectra (Fig. 5d). The two additional overlapping or hidden peaks at 2970 and 2880 cm^{-1} represent the asymmetric and symmetric CH$_3$ modes, respectively [71].

All three samples (Pt/KIT-6, Pt/SiO$_2$, and Pt/Al$_2$O$_3$) exhibited rela-tively analogous desorption properties, demonstrating that a significant quantity of MCH desorbs from the surface at 100 °C after 9 min of N$_2$ flushing over the catalyst. Complete MCH desorption was confirmed when the temperature increased to 200 °C. This indicates that the esti-mated adsorption strengths of MCH over all the samples were similar. The only evident difference was observed in the broader peak shape for the Pt/KIT-6 catalyst. The difference in the intensity ratio of the asym-metric CH$_2$ vibration relative to the symmetric CH$_2$ vibration for Pt/KIT-6, when compared with the other catalysts, is attributed to the signifi-cant contribution of the -CH$_3$ stretching vibrations (Fig. 5d). This is in good agreement with the high-intensity adsorption peak at approxi-mately 1452 cm^{-1} in the Pt/KIT-6 desorption spectra, which is reported as arising from the deformation vibrations of the -CH$_3$ group [72].

The hypothesis is that this apparent difference in the -CH$_3$ intensity is
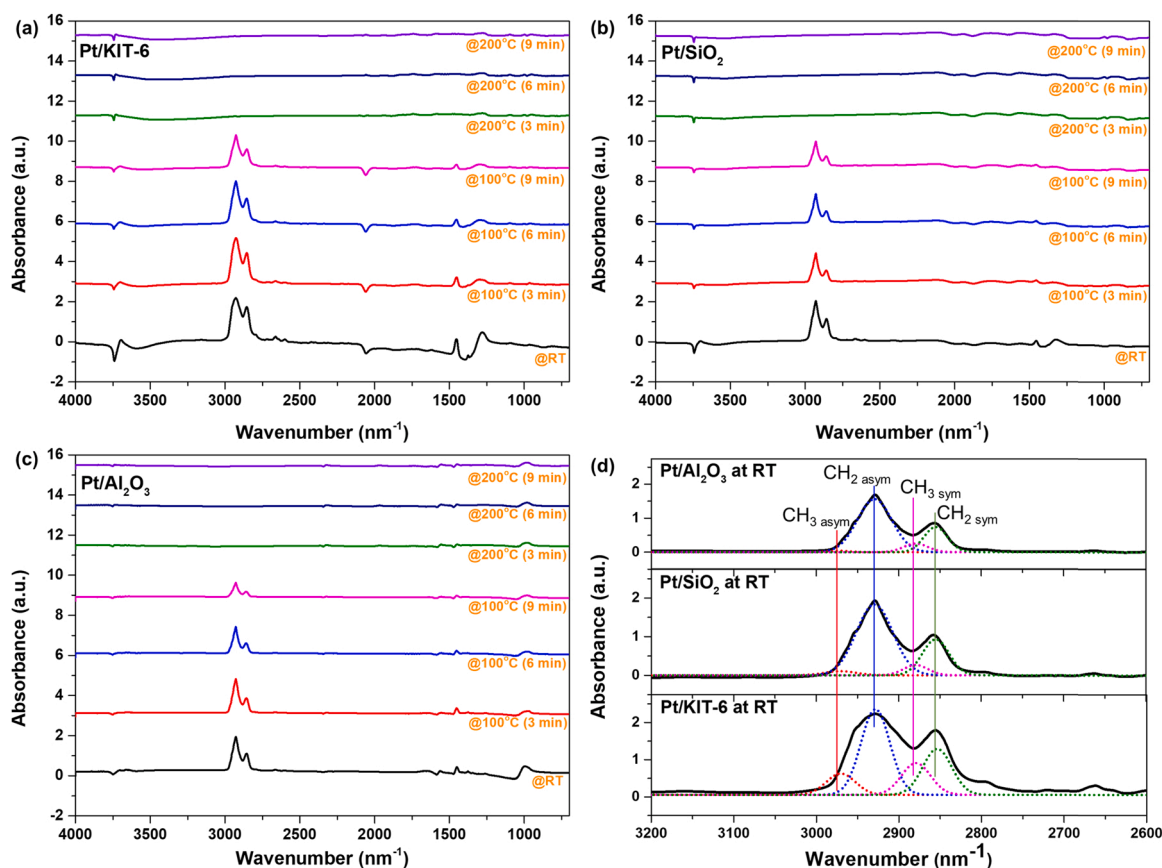
Fig. 5. *In situ* DRIFTS spectra of (a) Pt/KIT-6, (b) Pt/SiO₂, and (c) Pt/Al₂O₃ catalysts collected under MCH desorption conditions at varying temperatures. (d) Differences in the desorption spectra of the samples after N₂ flush at RT.

predominantly caused by the change in the adsorption structure at various adsorption sites. The MCH molecules can first approach the Pt catalyst surface in either a perpendicular orientation and/or a flat orientation [73]. With the first hydrogen abstraction, the C_7H_{13} species adsorbed on the Pt surface, and the structure changed depending on the position of the adsorbed carbon in the aromatic ring. Takise et al. [74] reported the optimized MCH adsorption structure and adsorption energy for MCH physisorption and chemisorption on the α, β, γ, and δ-carbon positions and methyl groups using DFT calculations. The authors state that γ and δ-carbon positions were more stable than the other positions, but the formation of all the adsorption structures was possible because the calculated adsorption energies were similar. Commensurate with their calculation results, it is highly possible that MCH adsorption in the methyl position (leading to CH_2) is significantly restricted for Pt/KIT-6 with the increasing pore-residence time attributed to the bicontinuous cubic mesoporous structure.

However, this noticeable difference in the -CH stretching intensities among the samples (Pt/KIT-6, Pt/SiO₂, and Pt/Al₂O₃) was eliminated when MCH was directly introduced at 300 °C (Fig. 6). The adsorption behavior at this high temperature (MCH dehydrogenation temperature) possibly leads to chemisorption at a similar position, while most of the unstable adsorption structures are not present on the catalyst surface. However, these structural differences in MCH chemisorption at RT are not directly related to the high catalytic activity of the Pt/KIT-6 catalyst, but strongly reflect the distinctiveness of the KIT-6 mesoporous matrix, resulting in a change in the adsorption behavior.

3.3.2.2. MCH adsorption at 300 °C. For this experiment, continuous MCH vapor was supplied for 1 h at 300 °C over the samples; the surface was then flushed with N₂ for an additional 30 min. Multiple spectra were collected during the adsorption and desorption of the MCH

molecules. The intensity of the peak indicating the quantity of adsorbed MCH (measured every 5 min) exhibited a marked increase for Pt/KIT-6 (Fig. 6). The maximum intensity of the overall -CHₓ stretching vibrations at the 60 min adsorption time, increased approximately 1.5–1.7 times in comparison with the other two catalysts: Pt/SiO₂ and Pt/Al₂O₃. The continuous increase in the surface concentration of MCH was attributed to the extended residence time inside the mesopores of the ordered structure of Pt/KIT-6. In contrast, the first adsorption spectra of the Pt/SiO₂ and Pt/Al₂O₃ samples reached the maximum intensity immediately and remained constant. Note that multiple spectra were collected and stacked onto each other in the figure. These results indicate that the surface concentration of MCH inside the Pt/SiO₂ and Pt/Al₂O₃ pore structures immediately reached equilibrium. The toluene adsorption peaks (C-H bond stretching) generated by MCH dehydrogenation were observed at around 3000–3150 cm⁻¹ in all cases [74]; the intensity of the doublet peaks was the highest for the Pt/KIT-6 catalyst. The order of increase in the intensity of these doublet peaks coincides with that of the increase in the catalytic activity for MCH dehydrogenation. This result indicates that part of the injected MCH vapor was successfully converted into toluene via dehydrogenation, and the in situ DRIFTS experimental conditions were similar to the actual reaction conditions.

The desorption of MCH after the termination of the MCH vapor supply was observed for 30 min (Fig. 6, red line). The adsorbed MCH molecules were rapidly desorbed at 300 °C, as expected. Only a small quantity of MCH remained on the catalyst surface at an early stage, but desorbed within 10 min for Pt/KIT-6 and Pt/SiO₂ (Fig. 6a and c). However, a longer desorption time was required for the complete desorption of MCH for Pt/Al₂O₃ (Fig. 6b). This suggests that MCH molecules were more tightly chemisorbed on the surface of Pt/Al₂O₃, primarily because of the high surface acidity of the support under the reaction conditions.
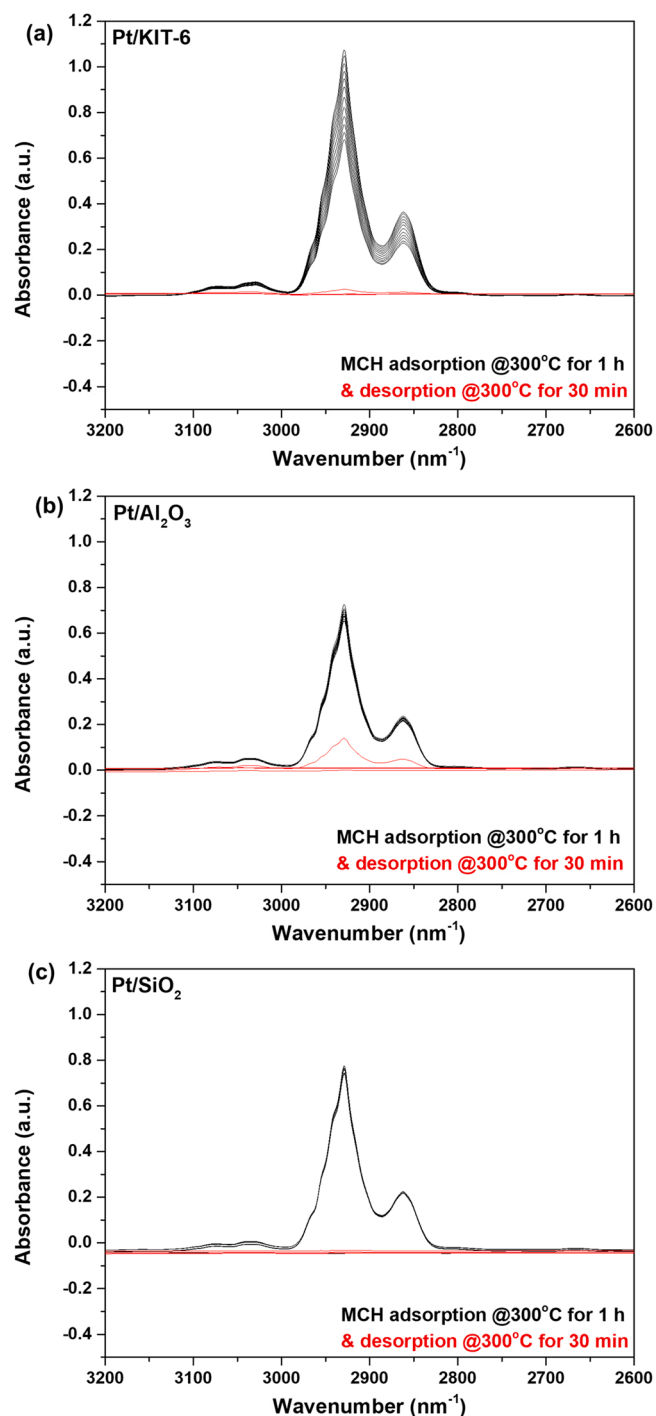
Fig. 6. *In situ* DRIFTS spectra of (a) Pt/KIT-6, (b) Pt/Al$_2$O$_3$, and (c) Pt/SiO$_2$ catalysts collected under MCH adsorption and desorption conditions at 300 ℃.

3.3.3. H12-BPDM dehydrogenation

Dehydrogenation of H12-BPDM was performed to clearly identify the structure-selectivity correlation in the Pt/KIT-6 catalyst. Overall, the catalytic activity and stability data shown in Fig. 7 agree well with the results from the MCH dehydrogenation: (1) Pt/KIT-6 exhibited the best dehydrogenation activities at all space velocity conditions (340 °C, 1 bar), and (2) the average DoDH values were in the order of Pt/KIT-6 > Pt/Al$_2$O$_3$ > Pt/SiO$_2$, and (3) high stability of Pt/KIT-6. The extent of

the decrease in activity with increasing LHSV values is the lowest for the Pt/KIT-6 catalyst, which is identical to the previous observation when tested for MCH dehydrogenation. These results indicate that the 3D mesoporous structure of KIT-6 has a strong promotion effect on the activity of the Pt/KIT-6 catalyst and indicates an increase in the pore-residence time within its support structure.

It should be noted that longer pore-residence may also lead to an inhibition effect attributed to the increase in product concentration near the Pt active sites. However, the readsorption of the dehydrogenated form of product molecules is not significant under the reaction conditions rather desorbs from the Pt/KIT-6 surface evidentially shown in the comparisons, which Pt/KIT-6 revealed significantly higher catalytic stability compared with the other two catalysts (Fig. 7a).

Detailed liquid product distributions were obtained (after 15 h of reaction) for the dehydrogenation of H12-BPDM (Table 2 and Fig. 7c). The hydrogenated form of BPDM (H-BPDM), which is a mixture of bicyclohexyl (BC) and dicyclohexylmethane (DCM), leads to a biphenyl (BP) and diphenylmethane (DM) mixture, which produces intermediates such as cyclohexylbenzene (CB) and cyclohexylmethylbenzene (CMB) via the dehydrogenation process [20,25]. For the Pt/KIT-6 catalyst, the sum of the compositions of the desired products (BP, DM) in the liquid phase was approximately 94%, which is significantly higher than that of Pt/SiO$_2$ and Pt/Al$_2$O$_3$. Fewer than 2% of the partially dehydrogenated products (CB and CMB) were present in the liquid phase, whereas the sum of the compositions of these by-products increased to 35% and 20% over the Pt/SiO$_2$ and Pt/Al$_2$O$_3$ catalysts, respectively. Overall, commensurate with the in situ DRIFTS and MCH dehydrogenation results, it can be concluded that the high BPDM selectivity might be attributed to the increase in the pore-residence time of the 3D mesoporous structure of KIT-6, leading to complete dehydrogenation of the H12-BPDM with minimal by-product formation.

In addition to the three catalyst supports selected for this study, SBA-15, which is one of the widely known ordered mesoporous silica with high specific surface area and regular 2D pore structure, was employed for Pt-based LOHC dehydrogenation catalyst to investigate whether the increase in catalytic activity and stability is predominantly attributed to the 3D pore structure of KIT-6. SBA-15 was synthesized by the self-assembly of copolymer micelles & hydrothermal method [75]. Pt of 1 wt% was impregnated on SBA-15 via wet impregnation approach and its catalytic activity was compared to the Pt/KIT-6 catalyst. It should be noted that all the chemical and physical properties are significantly similar between the Pt-KIT-6 and Pt-SBA-15 except that the Pt/KIT-6 catalyst has a 3D bicontinuous cubic helical structure (Fig. S2 and Table S1). For H12-BPDM dehydrogenation (Fig. S3), the results clearly indicate that the reactivity of Pt/KIT-6 is superior to Pt/SBA-15 at all LHSVs conditions tested at 340 ℃. These results strongly suggest that the 3D structure of Pt/KIT-6 facilitates the reactivity of dehydrogenation compared to a Pt supported on 2D structured OMS (Pt/SBA-15) through longer pore-residence time of the support matrix.

MCH dehydrogenation with Pt/SBA-15 was further conducted at identical reaction conditions (300 ℃, 1 bar, 5.4 mL/gcat/h) and the activity was evaluated along with the other four catalysts including a high surface area Pt/Al$_2$O$_3$ containing smaller Pt particles of 1–2 nm (Pt/KIT-6, Pt/SiO$_2$, Pt/Al$_2$O$_3$ and Pt/Al$_2$O$_3$-HS). In this case as well, similar trends were observed where Pt/KIT-6 showed better dehydrogenation activity and stability than all other four catalysts (Fig. S4, Fig. S5 and Fig. S6). The discussion of longer pore-residence time originating from the KIT-6 3D mesoporous structure correlated with the high conversion will be studied in our future work with a more detailed kinetic analysis; for example, longer pore-residence time increases the number of collisions between the reactants thereby resulting in a higher pre-exponential factor.
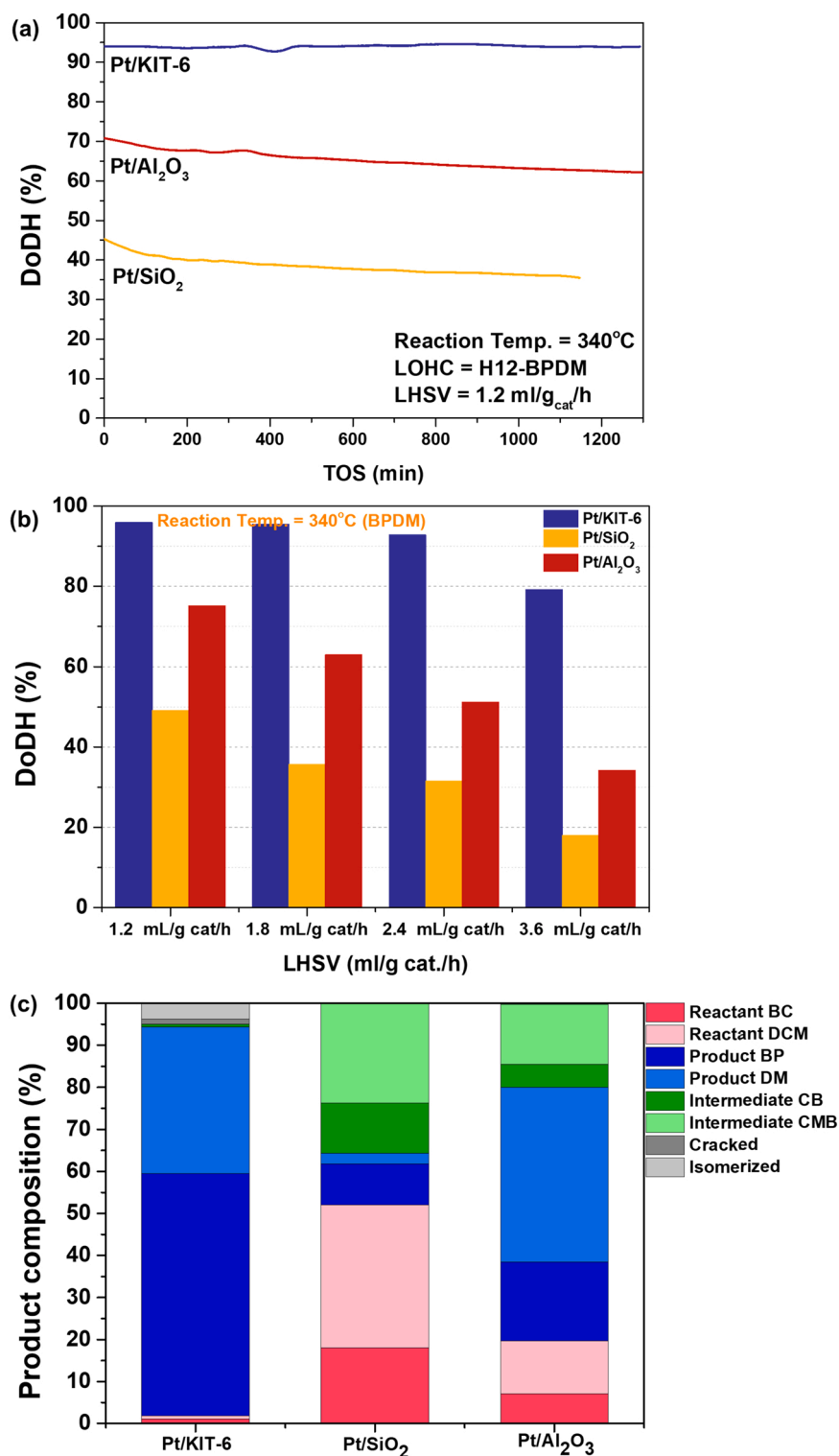
Fig. 7. Catalytic activity results for Pt/Al$_2$O$_3$, Pt/SiO$_2$, and Pt/KIT-6 catalysts under H12-BPDM dehydrogenation conditions: (a) Stability testing, (b) Reaction at varying LHSV values, and (c) Liquid product composition.

3.4. Post-catalysis analysis of tested catalysts

The STEM images of the post-catalysis samples were collected to identify the structural deformation of the catalysts and aggregation of Pt NPs (Fig. S7). Based on the Pt particle size distribution (Fig. S7), it was confirmed that the average particle size increased after the reaction for all samples. In particular, the particle size of Pt in the Pt/SiO$_2$ catalyst increased significantly. This is likely attributed to its low metal-support

interaction, where most of the Pt particles are mobile under the reaction conditions. Although the average particle sizes of the fresh and used catalysts were acquired from a different local area in the STEM analyses, it is noteworthy that Pt NPs distributed on the KIT-6 catalyst surface were evenly dispersed without significant aggregation and deformation of the well-developed mesoporous structure. Unlike Pt/SiO$_2$ and Pt/ Al$_2$O$_3$, the post-catalysis Pt/KIT-6 maintained narrow particle size distributions of 1–2 nm even after exposure to the H$_2$-rich and high-

Table 2
Liquid product composition obtained from dehydrogenation of H12-BPDM.

| Product		Pt/KIT-6	Pt/SiO$_2$	Pt/Al$_2$O$_3$
Reactant	Bicyclohexyl	1.01	18.02	7.07
Reactant	Dicyclohexylmethane	0.79	33.99	12.63
Product BP	Biphenyl	57.65	9.76	18.72
Product DM	Diphenylmethane	34.84	2.58	41.58
Intermediate CB	**Cyclohexyl-benzene**	**0.74**	**11.96**	**5.46**
Intermediate CMB	**Cyclohexylmethyl-benzene**	**0.01**	**23.56**	**14.28**
Cracked	Benzene + Toluene	1.17	0.10	0.05
Isomerized	9 H-Fluorene	3.79	0.02	0.22
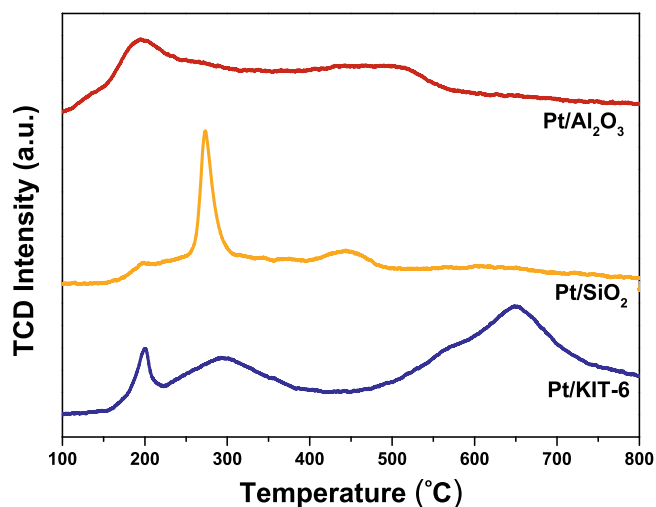
Fig. 8. TPO profiles of post-catalysis Pt/Al$_2$O$_3$, Pt/SiO$_2$, and Pt/KIT-6 catalysts.

temperature reaction conditions.

The specific surface area, total pore volume, and average pore diameter of the catalysts were analyzed post-catalysis, using N$_2$ isotherm curves (adsorption-desorption) and pore size distributions to determine the structural deformation during the dehydrogenation (Table S2 and Fig. S8). The surface area and total pore volume decreased after dehydrogenation. Similar to the STEM results, the average pore diameter between the as-prepared and post-catalysis samples of Pt/KIT-6 remained constant, indicating that the catalyst retained its specific 3-D regular mesoporous structure. This structural stability possibly affects the high stability of Pt/KIT-6, as indicated in the previous catalytic activity results.

Although surface coke formation was not observed in STEM images, the TPO thermograms of the post-catalysis samples (Fig. 8) revealed that a variety of coke species formed over Pt/KIT-6, Pt/SiO$_2$, and Pt/Al$_2$O$_3$. The samples were exposed to air prior to the data collection thus the contribution from Pt oxidation to the TCD signal was not significant. Overall, the peak at 200–500 °C represents an amorphous phase of the carbon deposit (soft coke). Amorphous coke containing a highly defective lattice structure is easily oxidized in those temperature range [76]. The presence of the filamentous coke (hard coke) phase [77], oxidized at 500–600 °C, was also confirmed. Moreover, graphitic coke was observed for Pt/KIT-6. Graphitic coke is highly crystalline and oxidizes at temperatures above 600 °C [78]. The noticeably broad peaks observed for Pt/KIT-6 and Pt/Al$_2$O$_3$ (the two most active catalysts) indicate the co-existence of different carbon allotropes, including amorphous, filamentous, and graphitic, on the catalysts. It should be noted that the coke formation is often significant for LOHC dehydrogenation because the products generally contain aromatic rings; thus, this does not only apply to the Pt/KIT-6 but to the catalysts with high dehydrogenation activity. In this study, although higher catalytic activity was observed for Pt/KIT-6, the catalyst was still significantly stable compared to the other

three catalysts.

4. Conclusion

The effect of using ordered mesoporous silica with a 3-D pore structure (KIT-6), as a Pt catalyst support, was investigated for the dehydrogenation of homocyclic LOHC (1: MCH, 2: hydrogenated biphenyl-based eutectic mixture (H-BPDM)). For both dehydrogenation reactions, Pt/KIT-6 exhibited significantly higher catalytic activity compared with that of Pt supported on disordered amorphous SiO$_2$ and Al$_2$O$_3$. The results of the H-BPDM dehydrogenation indicated the extremely low selectivity of the partially dehydrogenated products (by-products); cyclohexylbenzene (CB) and cyclohexylmethylbenzene (CMB) were obtained over the Pt/KIT-6 catalyst, whereas the selectivity increased significantly for Pt/SiO$_2$ and Pt/Al$_2$O$_3$.

The promising catalytic activity, product selectivity, and stability of Pt/KIT-6 can be attributed to its high surface area and pore volume. Furthermore, the Pt particles were more homogeneously dispersed on the KIT-6 support, resulting in a narrower particle size distribution and higher Pt dispersion. The calculated Pt average particle size was 1.3 nm. It was speculated that a longer pore-residence time was achieved because of the 3D bicontinuous pore structure of the Pt/KIT-6 catalyst, resulting in a higher concentration of the LOHC reactant near the Pt active sites. The longer pore-residence time originating from the KIT-6 structure correlated with the high conversion of LOHC and the product. This hypothesis was supported experimentally using the in situ DRIFTS technique, which revealed that a higher surface concentration of MCH was reached in a longer period over the Pt/KIT-6 catalyst surface in comparison with Pt/SiO$_2$ and Pt/Al$_2$O$_3$. Finally, post-catalysis analysis indicated that the ordered mesoporous structure of Pt/KIT-6 was maintained even after the reaction at high temperature. With respect to catalyst coking, all three samples exhibited deposition of different carbon species on the catalyst surface, and a higher concentration of graphitic coke was obtained for the Pt/KIT-6 catalyst.

CRediT authorship contribution statement

Chang-Il Ahn: Writing – original draft preparation. **Yeonsu Kwak:** Investigation, Writing. **Ah-Reum Kim:** Writing, Data curation. **Munjeong Jang:** XAS, Data curation. **Arash Badakhsh:** Writing, Data curation. **Junyoung Cha:** XAS, Data curation. **Yongmin Kim:** Validation. **Young Suk Jo:** Conceptualization. **Hyangsoo Jeong:** Supervision. **Sun Hee Choi:** Investigation. **Suk Woo Nam:** Conceptualization. **Chang Won Yoon:** Supervision, Writing – reviewing & editing. **Hyuntae Sohn:**

Writing – original draft preparation, Supervision.

Declaration of Competing Interest

The authors declare that they have no known competing financial interests or personal relationships that could have appeared to influence the work reported in this paper.

Acknowledgments

Appendix A. Supporting information

Supplementary data associated with this article can be found in the online version at doi:10.1016/j.apcatb.2022.121169.

References

[1] J.O. Abe, A.P.I. Popoola, E. Ajenifuja, O.M. Popoola, Hydrogen energy, economy and storage: review and recommendation, Int. J. Hydrog. Energy 44 (2019) 15072–15086, https://doi.org/10.1016/j.ijhydene.2019.04.068.

[2] M. Reuß, T. Grube, M. Robinius, P. Preuster, P. Wasserscheid, D. Stolten, Seasonal storage and alternative carriers: a flexible hydrogen supply chain model, Appl. Energy 200 (2017) 290–302, https://doi.org/10.1016/j.apenergy.2017.05.050.

[3] R.E. Rosli, A.B. Sulong, W.R.W. Daud, M.A. Zulkifley, T. Husaini, M.I. Rosli, E. H. Majlan, M.A. Haque, A review of high-temperature proton exchange membrane fuel cell (HT-PEMFC) system, Int. J. Hydrog. Energy 42 (2017) 9293–9314, https://doi.org/10.1016/j.ijhydene.2016.06.211.

[4] C.M. White, R.R. Steeper, A.E. Lutz, The hydrogen-fueled internal combustion engine: a technical review, Int. J. Hydrog. Energy 31 (2006) 1292–1305, https://doi.org/10.1016/j.ijhydene.2005.12.001.

[5] T. He, P. Pachfule, H. Wu, Q. Xu, P. Chen, Hydrogen carriers, Nat. Rev. Mater. 1 (2016), https://doi.org/10.1038/natrevmats.2016.59.

[6] P. Preuster, C. Papp, P. Wasserscheid, Liquid organic hydrogen carriers (LOHCs): toward a hydrogen-free hydrogen economy, Acc. Chem. Res. 50 (2017) 74–85, https://doi.org/10.1021/acs.accounts.6b00474.

[7] P.M. Modisha, C.N.M. Ouma, R. Garidzirai, P. Wasserscheid, D. Bessarabov, The prospect of hydrogen storage using liquid organic hydrogen carriers, Energy Fuels 33 (2019) 2778–2796, https://doi.org/10.1021/acs.energyfuels.9b00296.

[8] A.T. Wijayanta, T. Oda, C.W. Purnomo, T. Kashiwagi, M. Aziz, Liquid hydrogen, methylcyclohexane, and ammonia as potential hydrogen storage: comparison review, Int. J. Hydrog. Energy 44 (2019) 15026–15044, https://doi.org/10.1016/j.ijhydene.2019.04.112.

[9] S. Lee, G. Han, T. Kim, Y.S. Yoo, S.Y. Jeon, J. Bae, Connected evaluation of polymer electrolyte membrane fuel cell with dehydrogenation reactor of liquid organic hydrogen carrier, Int. J. Hydrog. Energy 45 (2020) 13398–13405, https://doi.org/10.1016/j.ijhydene.2020.02.129.

[10] Y. Okada, E. Sasaki, E. Watanabe, S. Hyodo, H. Nishijima, Development of dehydrogenation catalyst for hydrogen generation in organic chemical hydride method, Int. J. Hydrog. Energy 31 (2006) 1348–1356, https://doi.org/10.1016/j.ijhydene.2005.11.014.

[11] N. Boufaden, R. Akkari, B. Pawelec, J.L.G. Fierro, M. Said Zina, A. Ghorbel, Dehydrogenation of methylcyclohexane to toluene over partially reduced Mo-SiO2 catalysts, Appl. Catal. A Gen. 502 (2015) 329–339, https://doi.org/10.1016/j.apcata.2015.05.026.

[12] N. Boufaden, R. Akkari, B. Pawelec, J.L.G. Fierro, M.S. Zina, A. Ghorbel, Dehydrogenation of methylcyclohexane to toluene over partially reduced silica-supported Pt-Mo catalysts, J. Mol. Catal. A Chem. 420 (2016) 96–106, https://doi.org/10.1016/j.molcata.2016.04.011.

[13] N. Brückner, K. Obesser, A. Bösmann, D. Teichmann, W. Arlt, J. Dungs, P. Wasserscheid, Evaluation of industrially applied heat-transfer fluids as liquid organic hydrogen carrier systems, ChemSusChem 7 (2014) 229–235, https://doi.org/10.1002/cssc.201300426.

[14] H. Jorschick, M. Vogl, P. Preuster, A. Bösmann, P. Wasserscheid, Hydrogenation of liquid organic hydrogen carrier systems using multicomponent gas mixtures, Int. J. Hydrog. Energy 44 (2019) 31172–31182, https://doi.org/10.1016/j.ijhydene.2019.10.018.

[15] A.N. Kalenchuk, S.A. Chernyak, V.I. Bogdan, V.V. Lunin, Dehydrogenation of bicyclohexyl on a Pt catalyst based on oxidized carbon nanotubes, Dokl. Phys. Chem. 482 (2018) 121–124, https://doi.org/10.1134/S0012501618090014.

[16] D.H. Zaitsau, V.N. Emel'yanenko, A.A. Pimerzin, S.P. Verevkin, Benchmark properties of biphenyl as a liquid organic hydrogen carrier: evaluation of thermochemical data with complementary experimental and computational methods, J. Chem. Thermodyn. 122 (2018) 1–12, https://doi.org/10.1016/j.jct.2018.02.025.

[17] M. Amende, C. Gleichweit, K. Werner, S. Schernich, W. Zhao, M.P.A. Lorenz, O. Höfert, C. Papp, M. Koch, P. Wasserscheid, M. Laurin, H.P. Steinrück, J. Libuda, Model catalytic studies of liquid organic hydrogen carriers: dehydrogenation and decomposition mechanisms of dodecahydro-n-ethylcarbazole on pt(111), ACS Catal. 4 (2014) 657–665, https://doi.org/10.1021/cs400946x.

[18] Z. Jiang, S. Guo, T. Fang, Enhancing the catalytic activity and selectivity of PdAu/SiO2 bimetallic catalysts for dodecahydro- N-ethylcarbazole dehydrogenation by controlling the particle size and dispersion, ACS Appl. Energy Mater. 2 (2019) 7233–7243, https://doi.org/10.1021/acsaem.9b01202.

[19] D.J. Han, Y.S. Jo, B.S. Shin, M. Jang, J.W. Kang, J.H. Han, S.W. Nam, C.W. Yoon, A novel eutectic mixture of biphenyl and diphenylmethane as a potential liquid organic hydrogen carrier: catalytic hydrogenation, Energy Technol. 7 (2019) 113–121, https://doi.org/10.1002/ente.201700694.

[20] M. Jang, Y.S. Jo, W.J. Lee, B.S. Shin, H. Sohn, H. Jeong, S.C. Jang, S.K. Kwak, J. W. Kang, C.W. Yoon, A. High-Capacity, Reversible liquid organic hydrogen carrier: H 2 -release properties and an application to a fuel cell, ACS Sustain. Chem. Eng. 7 (2019) 1185–1194, https://doi.org/10.1021/acssuschemeng.8b04835.

[21] F. Auer, D. Blaumeiser, T. Bauer, A. Bösmann, N. Szesni, J. Libuda, P. Wasserscheid, Boosting the activity of hydrogen release from liquid organic hydrogen carrier systems by sulfur-additives to Pt on alumina catalysts, Catal. Sci. Technol. 9 (2019) 3537–3547, https://doi.org/10.1039/c9cy00817a.

[22] Y. Nakaya, M. Miyazaki, S. Yamazoe, K.I. Shimizu, S. Furukawa, Active, selective, and durable catalyst for alkane dehydrogenation based on a well-designed trimetallic alloy, ACS Catal. 10 (2020) 5163–5172, https://doi.org/10.1021/acscatal.0c00151.

[23] M. Kosaka, T. Higo, S. Ogo, J.G. Seo, S. Kado, K. Ichi Imagawa, Y. Sekine, Low-temperature selective dehydrogenation of methylcyclohexane by surface protonics over Pt/anatase-TiO2 catalyst, Int. J. Hydrog. Energy 45 (2020) 738–743, https://doi.org/10.1016/j.ijhydene.2019.10.133.

[24] M. Lersch, M. Tilset, Mechanistic aspects of C-H activation by Pt complexes, Chem. Rev. 105 (2005) 2471–2526, https://doi.org/10.1021/cr030710y.

[25] Y. Kwak, S. Moon, C. il Ahn, A.R. Kim, Y. Park, Y. Kim, H. Sohn, H. Jeong, S. W. Nam, C.W. Yoon, Y.S. Jo, Effect of the support properties in dehydrogenation of biphenyl-based eutectic mixture as liquid organic hydrogen carrier (LOHC) over Pt/Al2O3 catalysts, Fuel 284 (2021), 119285, https://doi.org/10.1016/j.fuel.2020.119285.

[26] F. Alhumaidan, D. Cresswell, A. Garforth, Hydrogen storage in liquid organic hydride: producing hydrogen catalytically from methylcyclohexane, Energy Fuels 25 (2011) 4217–4234, https://doi.org/10.1021/ef200829x.

[27] A. Shukla, S. Karmakar, R.B. Biniwale, Hydrogen delivery through liquid organic hydrides: considerations for a potential technology, Int. J. Hydrog. Energy 37 (2012) 3719–3726, https://doi.org/10.1016/j.ijhydene.2011.04.107.

[28] R.W. Coughlin, K. Kawakami, A. Hasan, Activity, yield patterns, and coking behavior of Pt and PtRe catalysts during dehydrogenation of methylcyclohexane. I. In the absence of sulfur, J. Catal. 88 (1984) 150–162, https://doi.org/10.1016/0021-9517(84)90060-5.

[29] M.R. Usman, D.L. Cresswell, A.A. Garforth, Selectivity of the formation of the ring-closed products and methylcyclohexenes in the dehydrogenation of methylcyclohexane to toluene, ISRN, Chem. Eng. 2012 (2012) 1–7, https://doi.org/10.5402/2012/818953.

[30] B. Liu, Z. Wang, Q. Zhu, X. Li, J. Wang, Performance of Pt/ZrO2–TiO2–Al2O3 and coke deposition during methylcyclohexane catalytic cracking, Fuel 200 (2017) 387–394, https://doi.org/10.1016/j.fuel.2017.03.058.

[31] M.R. Usman, D.L. Cresswell, A.A. Garforth, By-products formation in the dehydrogenation of methylcyclohexane, Pet. Sci. Technol. 29 (2011) 2247–2257, https://doi.org/10.1080/10916466.2011.584103.

[32] L. Bai, Y. Zhou, Y. Zhang, H. Liu, M. Tang, Influence of calcium addition on catalytic properties of PtSn/ZSM-5 catalyst for propane dehydrogenation, Catal. Lett. 129 (2009) 449–456, https://doi.org/10.1007/s10562-008-9822-9.

[33] F. Alhumaidan, D. Tsakiris, D. Cresswell, A. Garforth, Hydrogen storage in liquid organic hydride: selectivity of MCH dehydrogenation over monometallic and bimetallic Pt catalysts, Int. J. Hydrog. Energy 38 (2013) 14010–14026, https://doi.org/10.1016/j.ijhydene.2013.08.067.

[34] A. Nakano, S. Manabe, T. Higo, H. Seki, S. Nagatake, T. Yabe, S. Ogo, T. Nagatsuka, Y. Sugiura, H. Iki, Y. Sekine, Effects of Mn addition on dehydrogenation of methylcyclohexane over Pt/Al2O3 catalyst, Appl. Catal. A Gen. 543 (2017) 75–81, https://doi.org/10.1016/j.apcata.2017.06.017.

[35] Y. Tuo, Y. Meng, C. Chen, D. Lin, X. Feng, Y. Pan, P. Li, D. Chen, Z. Liu, Y. Zhou, J. Zhang, Partial positively charged Pt in Pt/MgAl2O4 for enhanced dehydrogenation activity, Appl. Catal. B Environ. 288 (2021) 119996, https://doi.org/10.1016/j.apcatb.2021.119996.

[36] S. Dürr, S. Zilm, M. Geißelbrecht, K. Müller, P. Preuster, A. Bösmann, P. Wasserscheid, Experimental determination of the hydrogenation/dehydrogenation - equilibrium of the LOHC system H0/H18-dibenzyltoluene, Int. J. Hydrog. Energy 46 (2021) 32583–32594, https://doi.org/10.1016/j.ijhydene.2021.07.119.

[37] X. Gong, Z. Jiang, T. Fang, Enhancing selectivity and reducing cost for dehydrogenation of dodecahydro-N-ethylcarbazole by supporting platinum on titanium dioxide, Int. J. Hydrog. Energy 45 (2020) 6838–6847, https://doi.org/10.1016/j.ijhydene.2019.12.203.

[38] A. Bulgarin, H. Jorschick, P. Preuster, A. Bösmann, P. Wasserscheid, Purity of hydrogen released from the liquid organic hydrogen carrier compound perhydro dibenzyltoluene by catalytic dehydrogenation, Int. J. Hydrog. Energy 45 (2020) 712–720, https://doi.org/10.1016/j.ijhydene.2019.10.067.

[39] E. Gianotti, M. Taillades-Jacquin, J. Rozière, D.J. Jones, High-purity hydrogen generation via dehydrogenation of organic carriers: a review on the catalytic process, ACS Catal. 8 (2018) 4660–4680, https://doi.org/10.1021/acscatal.7b04278.

[40] B. Wang, T. Yan Chang, Z. Jiang, J. Jia Wei, Y. Hai Zhang, S. Yang, T. Fang, Catalytic dehydrogenation study of dodecahydro-N-ethylcarbazole by noble metal supported on reduced graphene oxide, Int. J. Hydrog. Energy 43 (2018) 7317–7325, https://doi.org/10.1016/j.ijhydene.2018.02.156.

[41] X. Li, P. Shen, X. Han, Y. Wang, Y. Zhu, Z. Wu, Dehydrogenation mechanisms of liquid organic hydrogen carriers over Pt, Pd, Rh, and Ni surfaces: cyclohexane as a model compound, Appl. Surf. Sci. 543 (2021), 148769, https://doi.org/10.1016/j.apsusc.2020.148769.

[42] J. Zhou, J. Suk Chung, S. Gu Kang, Designing Pt-based subsurface alloy catalysts for the dehydrogenation of perhydro-dibenzyltoluene: a first-principles study, Appl. Surf. Sci. 579 (2021), 152142, https://doi.org/10.1016/j.apsusc.2021.152142.

[43] X. Chen, C.H. Gierlich, S. Schötz, D. Blaumeiser, T. Bauer, J. Libuda, R. Palkovits, Hydrogen production based on liquid organic hydrogen carriers through sulfur doped platinum catalysts supported on TiO2, ACS Sustain. Chem. Eng. 9 (2021) 6561–6573, https://doi.org/10.1021/acssuschemeng.0c09048.

[44] P.T. Aakko-Saksa, M. Vehkamäki, M. Kemell, L. Keskiväli, P. Simell, M. Reinikainen, U. Tapper, T. Repo, Hydrogen release from liquid organic hydrogen carriers catalysed by platinum on rutile-anatase structured titania, Chem. Commun. 56 (2020) 1657–1660, https://doi.org/10.1039/c9cc09715e.

[45] S. Lee, J. Lee, T. Kim, G. Han, J. Lee, K. Lee, J. Bae, Pt/CeO2 catalyst synthesized by combustion method for dehydrogenation of perhydro-dibenzyltoluene as liquid organic hydrogen carrier: effect of pore size and metal dispersion, Int. J. Hydrog. Energy 46 (2021) 5520–5529, https://doi.org/10.1016/j.ijhydene.2020.11.038.

[46] F. Auer, A. Hupfer, A. Bösmann, N. Szesni, P. Wasserscheidpeter, Influence of the nanoparticle size on hydrogen release and side product formation in liquid organic hydrogen carrier systems with supported platinum catalysts, Catal. Sci. Technol. 10 (2020) 6669–6678, https://doi.org/10.1039/d0cy01173h.

[47] L. Shi, Y. Zhou, S. Qi, K.J. Smith, X. Tan, J. Yan, C. Yi, Pt catalysts supported on H 2 and O 2 plasma-treated Al 2 O 3 for hydrogenation and dehydrogenation of the liquid organic hydrogen carrier pair dibenzyltoluene and perhydrodibenzyltoluene, ACS Catal. 10 (2020) 10661–10671, https://doi.org/10.1021/acscatal.0c03091.

[48] R. Garidzirai, P. Modisha, I. Shuro, J. Visagie, P. van Helden, D. Bessarabov, The effect of mg and zn dopants on pt/al2 o3 for the dehydrogenation of perhydrodibenzyltoluene, Catalysts 11 (2021) 1–20, https://doi.org/10.3390/catal11040490.

[49] J. Liang, Z. Liang, R. Zou, Y. Zhao, Heterogeneous catalysis in zeolites, mesoporous silica, and metal–organic frameworks, Adv. Mater. 29 (2017), https://doi.org/10.1002/adma.201701139.

[50] N. Linares, A.M. Silvestre-Albero, E. Serrano, J. Silvestre-Albero, J. García-Martínez, Mesoporous materials for clean energy technologies, Chem. Soc. Rev. 43 (2014) 7681–7717, https://doi.org/10.1039/c3cs60435g.

[51] J. Wei, Z. Sun, W. Luo, Y. Li, A.A. Elzatahry, A.M. Al-Enizi, Y. Deng, D. Zhao, New insight into the synthesis of large-pore ordered mesoporous materials, J. Am. Chem. Soc. 139 (2017) 1706–1713, https://doi.org/10.1021/jacs.6b11411.

[52] Y. Ren, Z. Ma, P.G. Bruce, Ordered mesoporous metal oxides: synthesis and applications, Chem. Soc. Rev. 41 (2012) 4909–4927, https://doi.org/10.1039/c2cs35086f.

[53] Y. Shi, Y. Wan, D. Zhao, Ordered mesoporous non-oxide materials, Chem. Soc. Rev. 40 (2011) 3854–3878, https://doi.org/10.1039/c0cs00186d.

[54] Y. Wan, D. Zhao, On the controllable soft-templating approach to mesoporous silicates, Chem. Rev. 107 (2007) 2821–2860, https://doi.org/10.1021/cr068020s.

[55] J. Zhu, T. Wang, X. Xu, P. Xiao, J. Li, Pt nanoparticles supported on SBA-15: synthesis, characterization and applications in heterogeneous catalysis, Appl. Catal. B Environ. 130–131 (2013) 197–217, https://doi.org/10.1016/j.apcatb.2012.11.005.

[56] D. Santhanaraj, C. Suresh, A. Selvamani, K. Shanthi, A comparison study between V-SBA-15 and V-KIT-6 catalysts for selective oxidation of diphenylmethane, New J. Chem. 43 (2019) 11554–11563, https://doi.org/10.1039/c9nj02007a.

[57] V. Chaudhary, S. Sharma, An overview of ordered mesoporous material SBA-15: synthesis, functionalization and application in oxidation reactions, J. Porous Mater. 24 (2017) 741–749, https://doi.org/10.1007/s10934-016-0311-z.

[58] M. Rezaei, A. Najafi Chermahini, H.A. Dabbagh, Green and selective oxidation of cyclohexane over vanadium pyrophosphate supported on mesoporous KIT-6, Chem. Eng. J. 314 (2017) 515–525, https://doi.org/10.1016/j.cej.2016.12.009.

[59] Y.S. Chen, Y.D. Cao, R. Ran, X.D. Wu, D. Weng, Controlled pore size of Pt/KIT-6 used for propane total oxidation, Rare Met. 37 (2018) 123–128, https://doi.org/10.1007/s12598-017-0937-2.

[60] Y. Cao, R. Ran, Y. Chen, X. Wu, D. Weng, Nanostructured platinum in ordered mesoporous silica as novel efficient catalyst for propane total oxidation, RSC Adv. 6 (2016) 30170–30175, https://doi.org/10.1039/C5RA27303J.

[61] C. Pirez, J.M. Caderon, J.P. Dacquin, A.F. Lee, K. Wilson, Tunable KIT-6 mesoporous sulfonic acid catalysts for fatty acid esterification, ACS Catal. 2 (2012) 1607–1614, https://doi.org/10.1021/cs300161a.

[62] R. Kishor, S. Bir, A. Kumar, ScienceDirect role of metal type on mesoporous KIT-6 for hydrogen storage, Int. J. Hydrog. Energy (2018) 2–11, https://doi.org/10.1016/j.ijhydene.2018.04.107.

[63] L. Deng, T. Arakawa, T. Ohkubo, H. Miura, S. Hosokawa, K. Teramura, T. Tanaka, Highly active and stable Pt-Sn / SBA-15 catalyst prepared by direct reduction for ethylbenzene dehydrogenation: Effects of Sn addition Highly active and stable Pt-Sn / SBA-15 catalyst prepared by direct reduction for ethylbenzene dehydrogenation: Effect, 2017.

[64] J.P.R. Alejandro, M.A.T. Sergio, S.A.J.G.A. Fuentes, U.A. De Sinaloa, J.O. De Domínguez, C. Universitaria, F.D.C.Q. Biológi-, Dehydrogenation of Propane to Propylene with Highly Stable Catalysts of Pt-Sn Supported Over Mesoporous Silica KIT-6 Abstract:, 2018, 1–10. https://doi.org/10.1515/ijcre-2017–0247.

[65] E.A. Martynenko, A.A. Pimerzin, A.A.P.A.A. Savinov, S.P. Verevkin, A.A. Pimerzin, E.A.M. Al, A.A.P.A.A. Savinov, S.P.V.A.A. Pimerzin, Hydrogen release from decalin by catalytic dehydrogenation over supported platinum catalysts, Top. Catal. 63 (2020) 178–186, https://doi.org/10.1007/s11244-020-01228-9.

[66] A. Hua Dong, K. Wang, S. Zhen Zhu, G. Bing Yang, X. Tao Wang, Facile preparation of PtSn-La/Al2O3 catalyst with large pore size and its improved catalytic performance for isobutane dehydrogenation, Fuel Process. Technol. 158 (2017) 218–225, https://doi.org/10.1016/j.fuproc.2017.01.004.

[67] M.Y. Kim, J.S. Choi, T.J. Toops, E.S. Jeong, S.W. Han, V. Schwartz, J. Chen, Coating SiO2 support with TiO2 or ZrO2 and effects on structure and CO oxidation performance of Pt catalysts, Catalysts 3 (2013) 88–103, https://doi.org/10.3390/catal3010088.

[68] C.A. Ignacio, V.Z. Armando, T. Viveros, Influence of the synthesis method on the catalytic behavior of pt and ptsn/Al 2O 3 reforming catalyst, Energy Fuels 23 (2009) 3835–3841, https://doi.org/10.1021/ef8010433.

[69] T.J. Rottreau, C.M.A. Parlett, A.F. Lee, R. Evans, Diffusion NMR characterization of catalytic silica supports: a tortuous path, J. Phys. Chem. C 121 (2017) 16250–16256, https://doi.org/10.1021/acs.jpcc.7b02929.

[70] G. Prieto, A. Martínez, R. Murciano, M.A. Arribas, Cobalt supported on morphologically tailored SBA-15 mesostructures: the impact of pore length on metal dispersion and catalytic activity in the Fischer-Tropsch synthesis, Appl. Catal. A Gen. 367 (2009) 146–156, https://doi.org/10.1016/j.apcata.2009.08.003.

[71] T. Elzein, A. Fahs, M. Brogly, A. Elhiri, B. Lepoittevin, P. Roger, V. Planchot, Adsorption of alkanethiols on gold surfaces: PM-IRRAS study of the influence of terminal functionality on alkyl chain orientation, J. Adhes. 89 (2013) 416–432, https://doi.org/10.1080/00218464.2013.757521.

[72] M.D. Hernández-Alonso, I. Tejedor-Tejedor, J.M. Coronado, M.A. Anderson, Operando FTIR study of the photocatalytic oxidation of methylcyclohexane and toluene in air over TiO2-ZrO2 thin films: influence of the aromaticity of the target molecule on deactivation, Appl. Catal. B Environ. 101 (2011) 283–293, https://doi.org/10.1016/j.apcatb.2010.09.029.

[73] W. Zhao, C. Chizallet, P. Sautet, P. Raybaud, Dehydrogenation mechanisms of methyl-cyclohexane on Γ-Al2O3 supported Pt13: impact of cluster ductility, J. Catal. 370 (2019) 118–129, https://doi.org/10.1016/j.jcat.2018.12.004.

[74] K. Takise, A. Sato, K. Murakami, S. Ogo, J.G. Seo, K.I. Imagawa, S. Kado, Y. Sekine, Irreversible catalytic methylcyclohexane dehydrogenation by surface protonics at low temperature, RSC Adv. 9 (2019) 5918–5924, https://doi.org/10.1039/c9ra00407f.

[75] S. Jun, Sang Hoon Joo, R. Ryoo, M. Kruk, M. Jaroniec, Z. Liu, T. Ohsuna, O. Terasaki, Synthesis of new, nanoporous carbon with hexagonally ordered mesostructure, J. Am. Chem. Soc. 122 (2000) 10712–10713, https://doi.org/10.1021/ja002261e, 5.

[76] K. Kamonsuangkasem, S. Therdthianwong, A. Therdthianwong, N. Thammajak, Remarkable activity and stability of Ni catalyst supported on CeO2-Al2O3 via CeAlO3 perovskite towards glycerol steam reforming for hydrogen production, Appl. Catal. B Environ. 218 (2017) 650–663, https://doi.org/10.1016/j.apcatb.2017.06.073.

[77] S.K. Sahoo, S.S. Ray, I.D. Singh, Structural characterization of coke on spent hydroprocessing catalysts used for processing of vacuum gas oils, Appl. Catal. A Gen. 278 (2004) 83–91, https://doi.org/10.1016/j.apcata.2004.09.028.

[78] K.Y. Koo, S.H. Lee, U.H. Jung, H.S. Roh, W.L. Yoon, Syngas production via combined steam and carbon dioxide reforming of methane over Ni-Ce/MgAl2O4 catalysts with enhanced coke resistance, Fuel Process. Technol. 119 (2014) 151–157, https://doi.org/10.1016/j.fuproc.2013.11.005.